remote sensing

MDPI

Article

Sea Surface Salinity Seasonal Variability in the Tropics from Satellites, in situ compilations and Mooring Observations

Frederick M. Bingham [1*], Susannah Brodnitz [2], and Lisan Yu[3]

[1] Center for Marine Science, University of North Carolina Wilmington, NC 28403-5928, USA; binghamf@uncw.edu
[2] University of North Carolina Wilmington; skbrodnitz@gmail.com
[3] Woods Hole Oceanographic Institution; lyu@whoi.edu
* Correspondence: binghamf@uncw.edu; Tel.: +1-910-962-2383

Received: date; Accepted: date; Published: date

Abstract: Satellite observations of sea surface salinity (SSS) have been validated in a number of instances using different forms of in situ data. One of the most energetic timescales of variability of SSS is the seasonal. Thus, it is important to know if satellites are getting the seasonal variability correct, and if the in situ products being used for validation are correct as well. In this study we validate SSS from satellite and in situ products using observations from moorings in the global tropical moored buoy array. We utilize 6 different satellite products, and two different in situ compilation products. For each product we have computed seasonal harmonics, including amplitude, phase and fraction of variance (R^2). These quantities are mapped for each product and for the moorings. We also do comparisons of amplitude, phase and R^2 between moorings and all the satellite and in situ products. Taking the mooring observations as ground truth, we find general good agreement between them and the satellite and in situ products, with near zero bias in phase and amplitude and small RMS differences. Tables are presented with these quantities for each product quantifying the degree of agreement.

Keywords: sea surface salinity, seasonal variability, satellite validation, harmonic analysis, mooring observations

1. Introduction

Sea surface salinity (SSS) has been observed by satellite for over 10 years since the launch of the SMOS (Soil Moisture and Ocean Salinity; [1]) instrument in 2009. Since then two other satellites have been launched by NASA that have measured SSS from space, Aquarius (2011-2015) [2] and SMAP (Soil Moisture Active Passive; 2015-present) [3]. Validation of these datasets has occurred in a number of contexts by comparison with in situ data [4-12]. Typically, individual satellite measurements are compared with nearby in situ measurements such as Argo floats [11], or more commonly with gridded Argo products such as that of [13] or the global HYCOM (Hybrid Coordinate Ocean Model) [3]. Problems exist with this type of comparison however. Individual float measurements are usually made at 5 m depth, and are spatially and temporally sparse compared to the satellite measurements. Gridded Argo products have their own uncertainty related to the sparse sampling and the gridding process [14].

In many regions of the ocean, the most important time scale is seasonal [15-20]. This is especially true in the tropics where the intertropical convergence zone (ITCZ) migrates seasonally in the meridional direction [21-23] bringing with it increased precipitation [24] and the seasonal translation of the North Equatorial Countercurrent front. Thus, SSS has been observed to have large seasonal variations in the tropics, especially north of the equator in the Pacific and Atlantic basins [16, 20, 25, 26] where the ITCZ is present and as a result of strong river discharge into the tropical Atlantic.

The global tropical moored buoy array (GTMBA) is a vast network of moorings stretching across all the ocean basins (Figure 1). It was set up starting in the 1980's to measure variations related to El Niño in the Pacific, but has since expanded to the Indian and Atlantic basins. (See https://www.pmel.noaa.gov/gtmba/ and [27] for a history of the program in the three different basins, and www.tpos2020.org for a discussion on the future of the Pacific portion of the array.) These moorings measure quantities such as wind, precipitation, humidity, currents, sea surface temperature, subsurface temperature, and, most importantly for the current study, SSS. The high quality standards, long record duration (some over 20 years – Figure 1) and location of the buoys in this array make them ideal platforms for validating satellite SSS measurements. Indeed, some of this is done by [5, 7, 28, 29] among others. However, to date there has been little explicit comparison of mooring and satellite SSS data at the seasonal time scale. [15] used the mooring data to compute annual harmonics, but made no comparison to satellites as such data did not exist at the time.

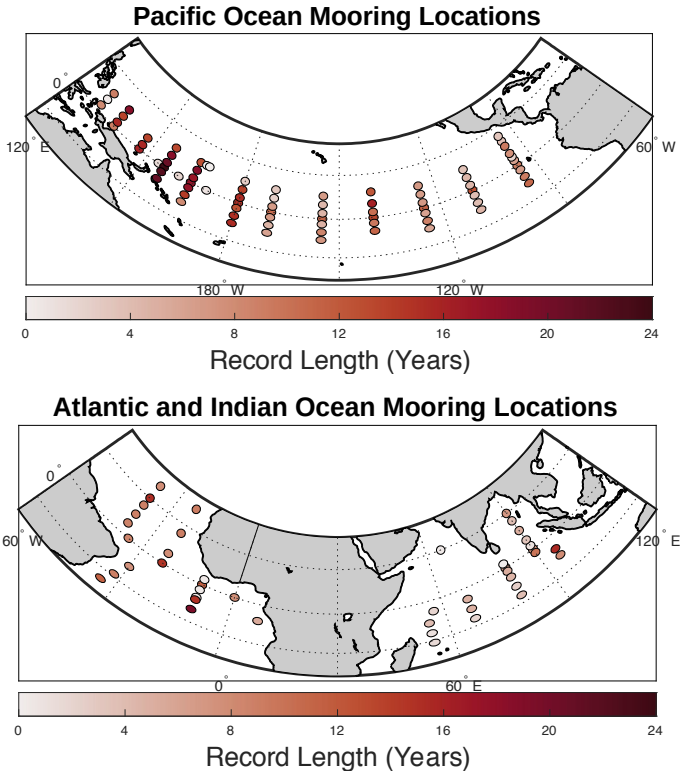

Figure 1. The Global Tropical Moored Buoy Array. (a) The array is called "TAO" in the eastern and central Pacific, "TRITON" in the western Pacific, (b) "PIRATA" in the Atlantic and "RAMA" in the Indian ocean. Note, some sites are not currently operational, especially in the western Pacific. Symbol colors correspond to the length of the record in years, with a scale at the bottom. The record length refers to the total number of hourly measurements regardless of gaps.

[19] found that a decorrelation scale of 80-100 days, corresponding to the seasonal time scale, was the most important one for about 1/3 of the global ocean, and that it was concentrated in the tropics. [15,16] using sparse historic and early Argo data found large amplitude seasonal harmonics in the tropical oceans. This result was verified by comparison to GTMBA data from the Pacific basin available at the time. Such large amplitude seasonal harmonics were also found by [17]and [18]. The most recent estimates of [18] using multiple satellite datasets found typical seasonal amplitudes of up to 0.5 in the tropics, with higher values in regions such as the Amazon and Congo River plumes.

We use data from the three satellites mentioned above: SMOS, SMAP and Aquarius. Although they use the same frequency of radiation to make their estimate, the satellites have very different configurations and ways of forming an image to retrieve values of SSS. Thus, we use two different level 3 SMOS products, one level 4 synthesis product, one Aquarius product, and two SMAP products. The various products have different ways of averaging or interpolating to get to a final version. Finally, we also examine two commonly used in situ gridded products. These compilations serve as calibration points or first guess fields used in the retrieval process for some of the satellite products [30]. In this paper we will directly compare all of these products to the mooring data at the seasonal time scale, and inter-compare two L3 SMOS and two SMAP products using the same methods. Comparison of these satellite and in situ datasets at the seasonal time scale is an important missing piece in the validation of satellite SSS [18].

2. Data and Methods

As stated above, we make use of 9 main SSS datasets, two in situ gridded (EN4 and SIO), one in situ moored and 6 satellite (Table 1). Table S1 extends Table 1 to give references where details of the methods used to generate the datasets can be found along with information for accessing all datasets.

Table 1. A list of the datasets used in this study showing the time resolution, spatial grid and time span.

Dataset	Time resolution	Spatial grid	Time span
Moorings	Hourly	N/A	various
SMOS BEC	Daily values with a 9-day running mean	0.25°	2011-2019
SMOS CATDS	4-day values with a 9-day running mean	Lon: 0.2594° Lat: varies from 0.1962° to 1.5341°	2010-2019
CCI	Daily values with a 7-day running mean	Lon: 0.2594° Lat: varies from 0.1962° to 1.5341°	2010-2018
SMAP JPL	8-day running mean	0.25°	2015-2020
SMAP RSS (70 km)	8-day running mean	0.25°	2015-2020
Aquarius	Daily	1°	2011-2015
EN4	Monthly	1°	2000-2018

SIO	Monthly	1°	2004-2020

Annual and semiannual harmonic fits were computed for each mooring time series following [18] and [15], and for each of the other products at the closest gid node to each mooring site. These computations yield amplitudes, phases (month of maximum SSS) and fractions of variance (R^2) associated with both annual and semiannual. We show results for the annual harmonics only in this paper. Semiannual harmonic amplitudes were generally smaller and we omit those results for brevity here, but include some of them in the supplemental materials.

Significance tests for the harmonic fits were carried out for the first and second harmonics separately. The R^2 value of each harmonic was calculated with the standard formula

$$R^2 = 1 - \frac{variance(data - fit)}{variance(data)}. \quad (1)$$

The f-statistic was then calculated from R^2 using the equation

$$f = \left(\frac{R^2}{1 - R^2}\right) \cdot \left(\frac{n - k - 1}{k}\right), \quad (2)$$

Where n is the number of observations (non-null data points in the time series at that location) and k is the number of independent variables, two in the case of looking at the annual and semiannual harmonics individually. Then the cumulative F-distribution function was used on the given f-statistic, n, and k, and fits with values greater than 0.95 were considered significant. The significance was calculated as if all the data points were independent observations. In addition to filtering by significance, we only considered locations where we had at least one year total of data points for a given data set.

In comparing the amplitudes, phases and R^2 values between mooring and products, we used the entirety of each dataset, including possibly non-overlapping periods. This was done because: 1) the computed amplitudes and phases seemed stable as described below, 2) we wanted to increase the significance of the computed fits, and 3) many of the moorings were sampled sporadically (e.g. Figure 2a) making determination of overlapping periods computationally cumbersome.

As an illustration of the method, we show the mooring data, harmonic fit, SIO data and its fit at the mooring site at (0°N, 0°E). Although there are large gaps in the mooring record (Figure 2a), a major advantage of the harmonic method is that it can make use of such time series. A possible problem with the method is if the amplitude or phase of the seasonal variability changes over time. The SIO data indicate that for this location this is not an issue (Figure 2b). The seasonal maximum or minimum does vary from year to year, but not in a systematic or interannual way. The signal appears phase-locked to the calendar year. The harmonic fits we have done do not depict some of the extreme events in the mooring record (Figure 2c), so in this sense it acts as a low pass filter. These low SSS events may indicate real events (e.g. [31]). The way they are displayed in the figure tends to exaggerate their importance however, as they generally consist of only a small number of hourly observations. The amplitudes of the two records in Figure 2a-c are similar. The peak-to-peak amplitude of the SIO fit is about 0.8 (Figure 2b), whereas that for the mooring is a little larger, about 1.0 (Figure 2c).

We also show data from a location in the eastern tropical North Pacific (Figure 2d; 10°N, 95°W). There is no fit displayed, but it is clear there is a large annual cycle in all the datasets. The amplitude and phase of that annual cycle is relatively stable,

except for 2015-2016. That change is likely associated with the El Niño event that occurred at that time.

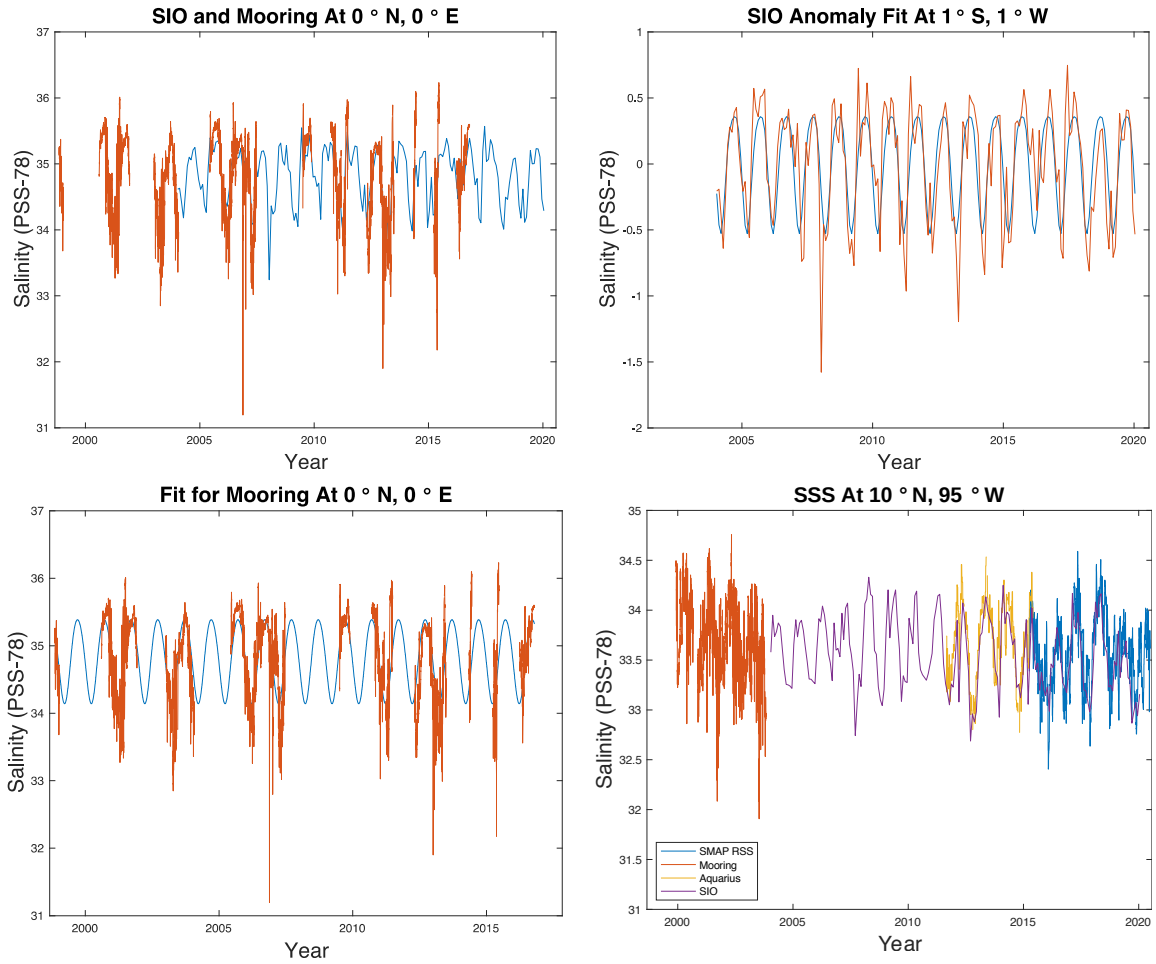

Figure 2. Harmonic fits and observations of SSS at (0°N, 0°E). (a) Mooring (red) and SIO (blue) observations. (b) SIO anomaly (red) and its harmonic fit (blue). (c) Mooring (red) and its harmonic fit (blue). (d) SSS data from 10°N, 95°W. Source of data is indicated in the legend at the bottom left.

3. Results

3.1 Amplitude and phase maps

The annual harmonics for the moorings (Figure 3) indicate a variety of amplitudes and phases. The largest amplitude, ~1.0, is near the west coast of Africa in the vicinity of the outlet of the Congo River. Other areas with large amplitude are in the Amazon River outflow in the western Atlantic, the western tropical Indian Ocean south of the equator, and along 10°N in the North Pacific. The sizes of the harmonics shown match well with the values reported by [15-18] among others. Phases show maximum SSS in the northern hemisphere mostly in December-January and in the southern hemisphere in July-August. The main exception to this is in the Bay of Bengal, with maximum SSS there in June.

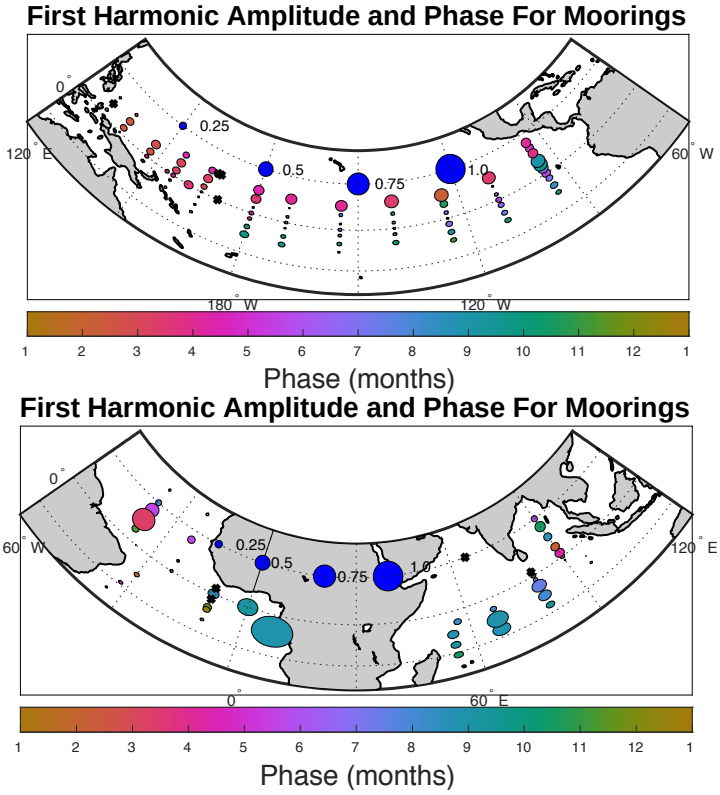

Figure 3. Amplitude and phase of the first harmonic from the moorings. Each symbol is for one mooring at its given location. The amplitude is indicated by the area of the symbol, with scale in dark blue near the top middle of each figure. The color of each symbol indicates the phase, as the month of maximum SSS, with color scale in months (January-January) at the bottom. Symbols with a black "X" were either found not to have a significant fit to the annual harmonic, or contained less than one year of observations. The maps use an equal area conic projection. This means that though the symbols change in shape from north to south, the relative areas are depicted correctly in relation to the dark blue scale. **(a)** Pacific basin. **(b)** Atlantic and Indian basins. For completeness, we include maps of amplitude and phase for all products for both annual (Table S2) and semi-annual (Table S5) harmonics.

Next, we show maps of fraction of variance, R^2, explained by the harmonic fit (Figure 4). In the Pacific basin, the numbers tend to be larger, over 0.5, in the ITCZ, in the western Pacific and south of the equator in the eastern Pacific, whereas they are small along the equator. In the Atlantic all the values are large, especially near the coast of Africa. In the Indian basin, the values get very large, approaching 1 in the western South Indian. All of these results indicate that in many areas, the seasonal time scale represents a large fraction of the total signal [18,19].

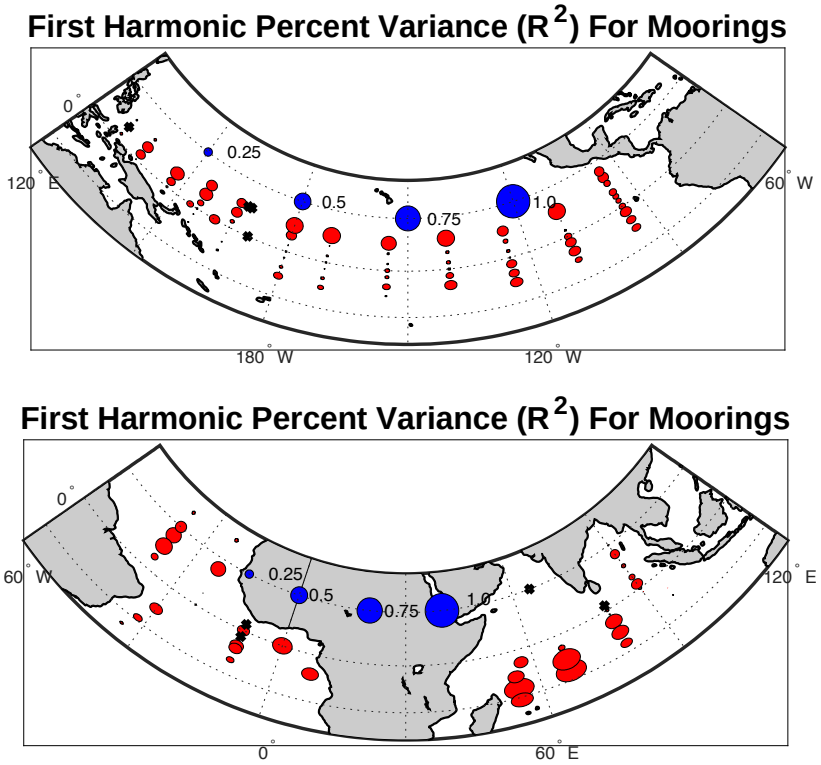

Figure 4. As in Figure 3, but for fraction of variance, R^2, explained by the annual harmonic fit. For completeness, we include maps of R^2 for all products for both annual (Table S3) and semi-annual (Table S6) harmonics.

The results presented in Figures 3 and 4 for the GTMBA are consistent with previous such calculations [15-17] using different datasets or [18] using mostly the same datasets. What we do differently here is to compare the various datasets against the moorings as ground truth, and to some extent each other. Analyses such as those of Figures 3 and 4 were carried out for all the different datasets mentioned in section 2. We present a couple of examples similar to Figure 3 here and a more complete set of them in the supplemental materials.

The RSS SMAP amplitude and phase (Figure 5) are similar to the moorings with a few minor differences. In the western Pacific along the equator, the SMAP RSS data show phase with maximum SSS in October, whereas in the mooring data those maxima are in December or so. The amplitudes are not large which may explain the difference. More of the SMAP RSS locations are below significance level than the moorings, especially off the equator in the central Pacific, likely due to the shorter record length. In the Atlantic and Indian basins, the results are also similar to the moorings. The results for R^2 are also very similar, and are not included here for brevity, but are in the supplemental materials (Table S3).

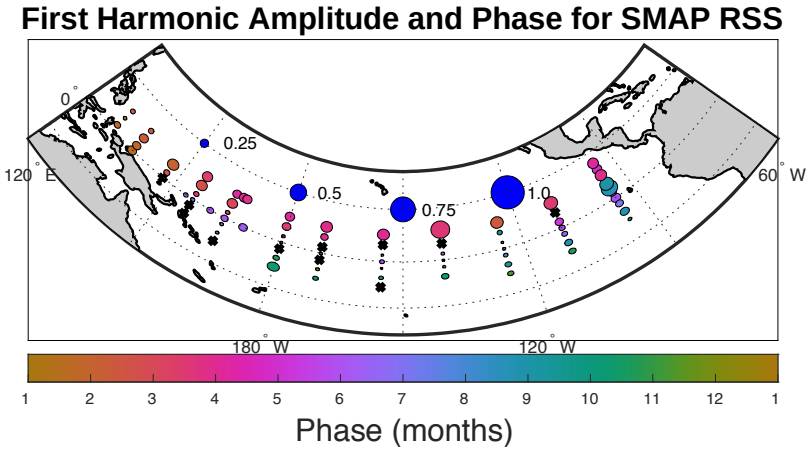

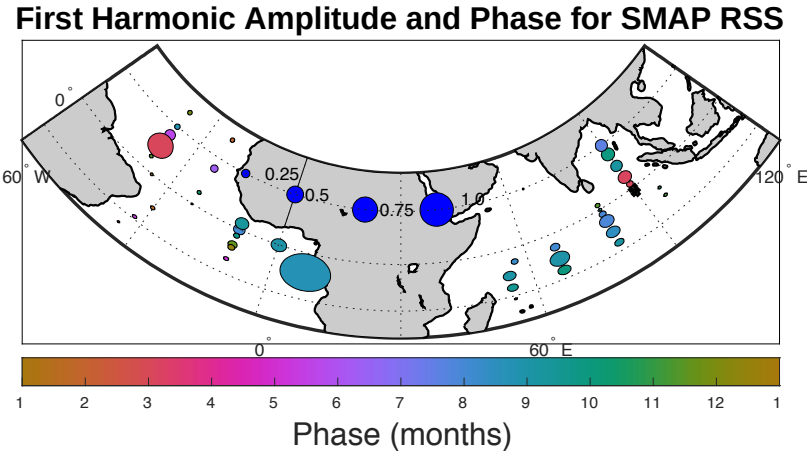

Figure 5. As in Figure 3, but for the SMAP RSS data.

The similarity of the mooring and SMAP RSS results is striking, and is repeated for most of the other datasets we analyzed (Tables S3 and S4). One exception is the SMOS BEC results shown in Figure 6. In this case there are major differences between these and the mooring data. The amplitudes are in general much smaller in the SMOS BEC data throughout the tropical ocean. Detailed comparison of the amplitudes and phases between the products is presented below as a set of scatter plots and RMS differences.

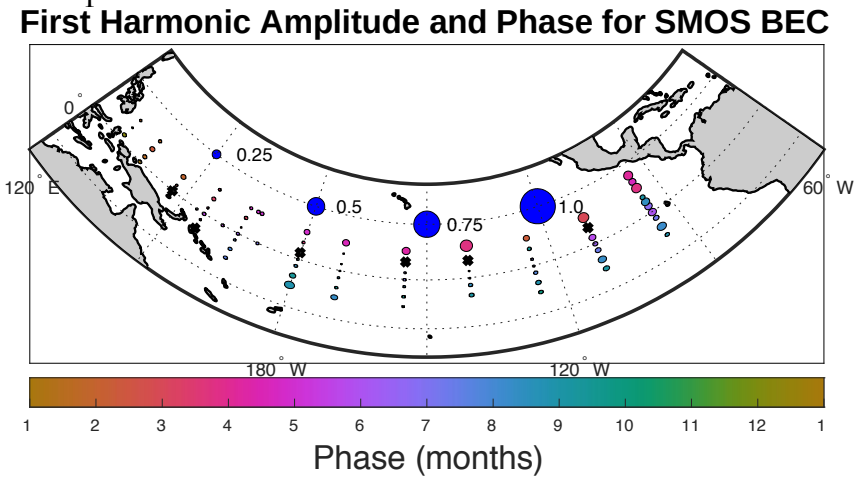

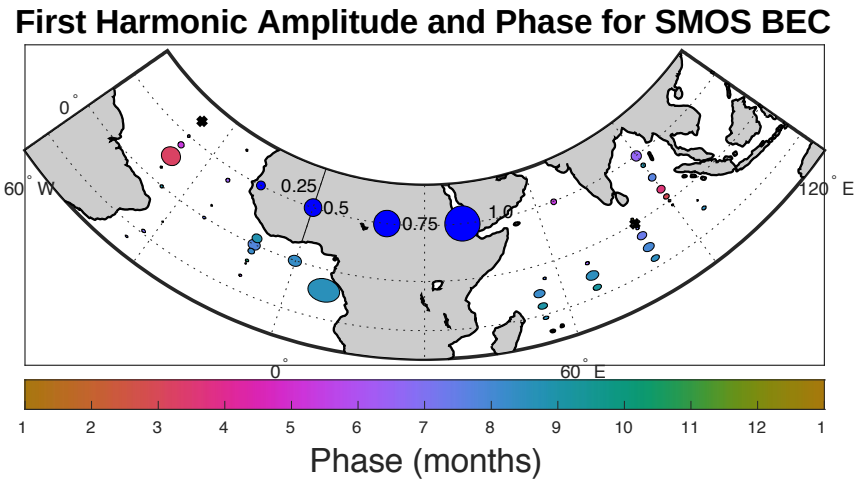

Figure 6. As in Figure 3, but for the SMOS BEC data.

3.2 Amplitude and phase comparisons

Comparison between mooring phases and the other datasets (Figure 7) show they mostly match well. Maximum SSS along the equator and at the southern hemisphere moorings is in mid-year, June-September, while for the northern hemisphere moorings it is in November-March. There is some tendency for small amplitude locations to be further off the one-to-one correspondence line than large amplitude ones. RMS differences (RMSD) between mooring and product phase range from 0.5 to 1.5 months, all significantly different from zero (Table 1). Median differences are all less than or equal to 0.1 in absolute value and none of them are significantly different from zero. The datasets with the largest scatter are the two SMAP datasets (Figure 7a,b; 1.3 months RMSD), Aquarius (Figure 7c; also 1.3 months) and SMOS BEC (Figure 7f; 1.5 months). The ones with the smallest scatter are the CCI (Figure 7d) and the two in situ datasets (Figure 7g,h), all with about 0.5 months RMSD.

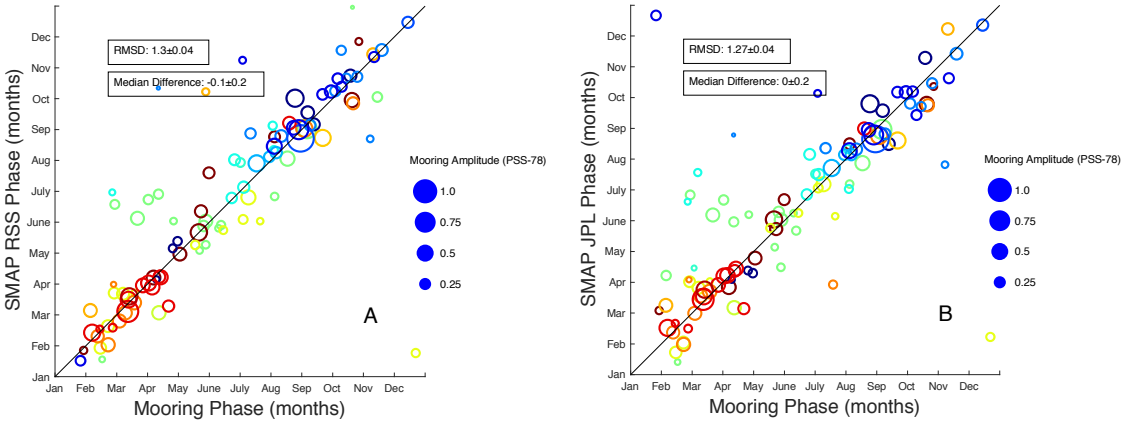

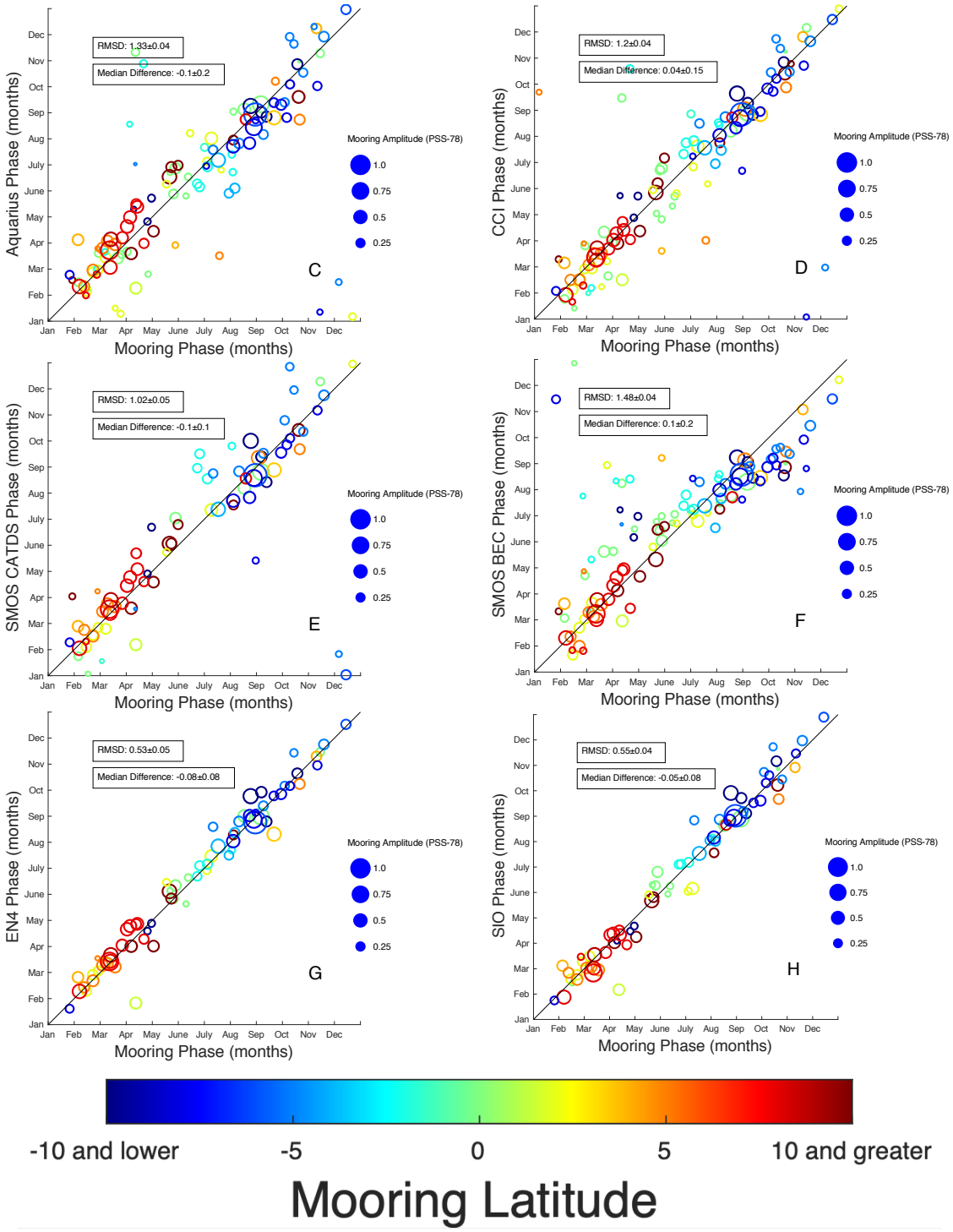

Figure 7. Scatterplots of first harmonic comparison product phase (month of maximum SSS) vs. mooring phase. Each symbol is for one mooring, with symbols plotted only where there is a significant annual fit for both the moorings and the given product. The number of symbols in each plot is given for each product in Table S7. Colors of symbols indicate latitude of mooring with scale at bottom. Sizes of symbols indicate mooring amplitude with scale at right in each panel. A light black line shows a one-to-one correspondence. Boxes in each panel show RMSD and median difference (mooring – comparison) in months. Products compared are: a) SMAP RSS, b) SMAP JPL, c) Aquarius, d) CCI, e) SMOS CATDS, f) SMOS BEC, g) EN4, h) SIO.

Table 2. Columns 2-5: Amplitude and phase discrepancies between mooring and satellite or in situ products. Median differences are mooring – product. Column 6: Median difference in R^2 between

mooring and satellite or in situ product for the annual harmonic. Positive number means mooring R^2 is greater.

Product	Amplitude RMSD	Phase RMSD (months)	Amplitude median difference	Phase median difference (months)	R^2 median difference
SMOS BEC	0.128±0.002	1.48±0.04	0.06±0.01	0.1±0.2	0.03
SMOS CATDS	0.085±0.004	1.02±0.05	0.01±0.01	-0.1±0.1	0.05
CCI	0.074±0.002	1.2±0.04	0.02±0.01	0.04±0.15	0.01
SMAP JPL	0.074±0.003	1.27±0.04	-0.013±0.009	-0.0±0.2	0.01
SMAP RSS	0.070±0.003	1.30±0.04	0.003±0.009	-0.1±0.2	0.01
Aquarius	0.108±0.003	1.33±0.04	-0.02±0.01	-0.1±0.2	-0.12
EN4	0.082±0.008	0.53±0.05	0.01±0.01	-0.08±0.08	-0.14
SIO	0.080±0.008	0.55±0.04	0.01±0.01	-0.05±0.08	-0.14

In a couple of cases we can compare two products whose underlying measurement is the same. There are two different L3 SMAP products and two L3 SMOS products (Figure 8). So, in making these comparisons, all of the difference between them is due to the processing algorithm and not the measurement platform. The SMAP products compare very well, with an RMSD of about 0.7 months and median difference not significantly different from zero (Figure 8a). The one outlier point is at (15°N, 65°E) in the Arabian Sea. (This harmonic is not included in any mooring plot because there are too few data at this location.) The two SMOS products do show some differences, with the SMOS BEC product generally leading the SMOS CATDS (Figure 8b). The median difference is 0.4 months.

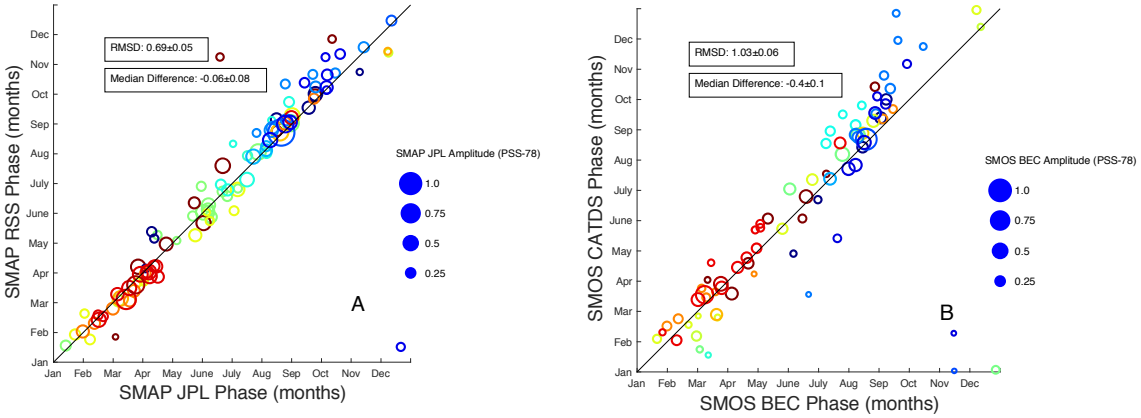

Figure 8. As in Figure 7. Comparisons are a) SMAP RSS vs. SMAP JPL and b) SMOS CATDS vs. SMOS BEC.

With the first harmonic amplitudes, we find that most satellite and in situ products compare well with the moorings (Figure 9 and Table 2). RMSDs are

typically 0.07-0.08 and median differences of about 0.01-0.03. The two exceptions are Aquarius, with RMSD of 0.11 and SMOS BEC with RMSD of 0.13. For the SMOS BEC dataset, the mooring amplitudes are generally larger than in the satellite data, with median difference of about 0.06.

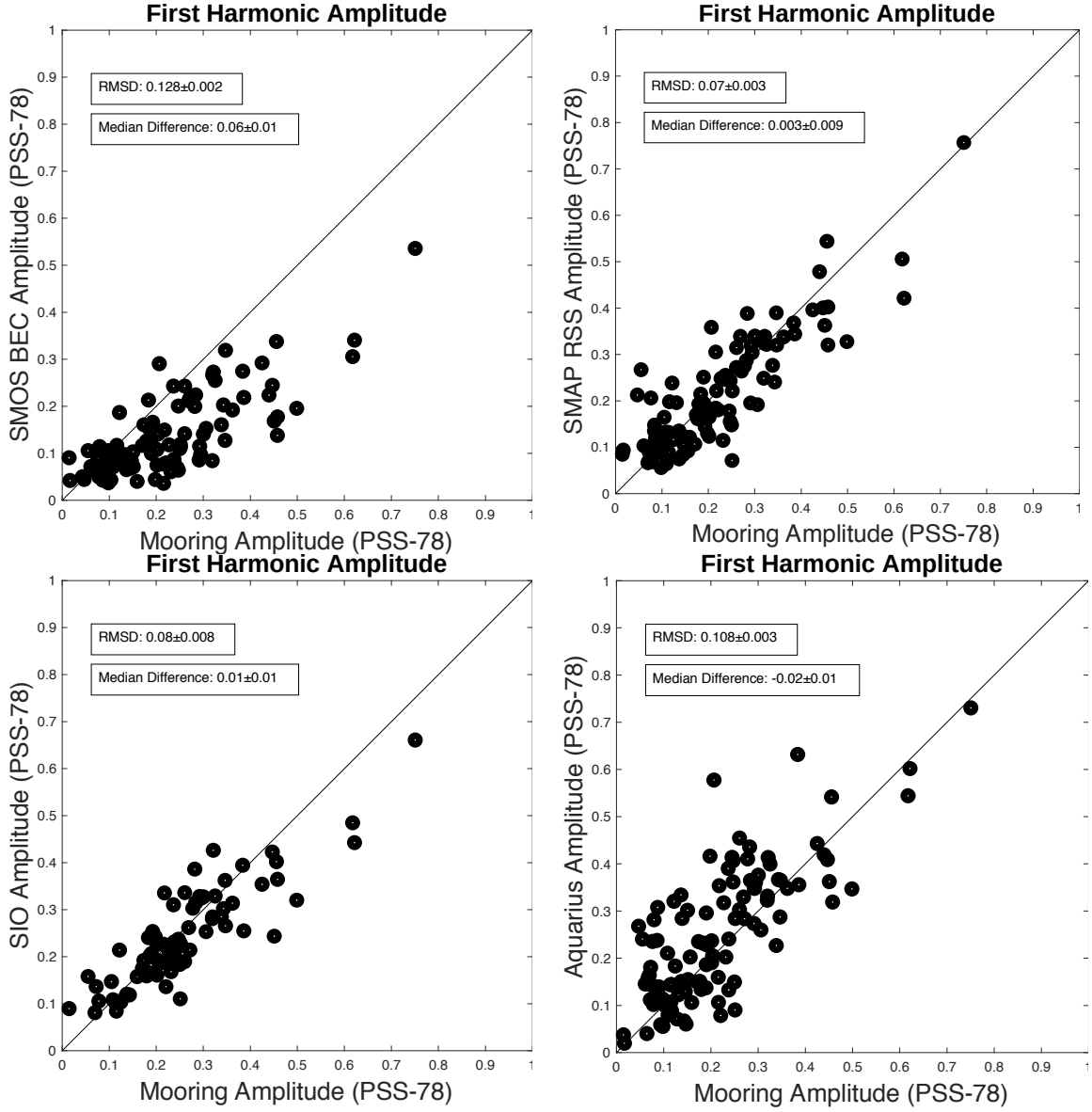

Figure 9. Scatterplots of first harmonic amplitude vs. mooring amplitude. A light black line shows a one-to-one correspondence. Boxes in each panel show RMSD and median difference (mooring – comparison). Comparison amplitudes are: a) SMOS BEC, b) SMAP RSS, c) SIO, d) Aquarius. For completeness, all first harmonic amplitude comparisons are shown in the supplemental materials (Table S4).

Table 2 shows the median of the difference between R^2 values for the mooring and that of the various products. In other words, for each dot in Figure 9, one can subtract the mooring value from the comparison product value, to obtain the degree to which those dots depart from the one-to-one line. One can then compute the median of those differences, to get the numbers displayed in Table 2. Table 3 shows the median over the dots for, say, the moorings or SMAP RSS. These values show which products tend to have large or small values of R^2.

An example set of R^2 comparisons are shown (Figure 10; Table 3). The value of R^2 is a function of the sampling of each dataset, as well as the amount of variance

each dataset may capture. Overall, in the tropics the annual harmonic only comprises about 20% of the total variance of SSS for the moorings. The moorings, one assumes as they are sampled hourly, capture all or almost all of the temporal variance in nature. The in situ datasets (EN4 and SIO) are averaged monthly and over a 1°X1° area, so any variance with smaller time and space scales is not present in those datasets. Thus, one would expect R^2 in the annual harmonic would be larger for these than for the moorings, which it is (Figure 10c; Table 3). For Aquarius, the issue is similar. It has a similarly large footprint, though with weekly time resolution (Table 1). Thus, it does not sample most of the variability at less than ~100 km in size. As much of ocean SSS variance is at sizes less than 50 km [32], the Aquarius dataset will miss it, and therefore, the annual harmonic will be a larger fraction of the variance than for the moorings (Figure 10d; Table 3). As we have seen, the SMOS BEC data underestimate the size of the annual harmonic, and so the fraction of variance captured in that dataset is less than for the moorings (Figure 10a; Table 3). Finally, the SMAP RSS product (Figure 10b; Table 3) has a smaller footprint than Aquarius, and more frequent sampling than SIO. The fraction of variance depicted in that dataset is comparable to that of the moorings. The datasets not plotted in Figure 10, SMOS CATDS, SMAP JPL, EN4 and CCI, all show similar patterns as SMAP RSS(Table 2).

Table 3. Median R^2 over all the mooring locations for all the products for the annual harmonic. The number of mooring locations used in each of these values is listed in Table S7.

	Median R^2
Moorings	0.190
SMOS BEC	0.103
SMOS CATDS	0.187
CCI	0.1842
SMAP JPL	0.198
SMAP RSS	0.203
Aquarius	0.316
EN4	0.351
SIO	0.430

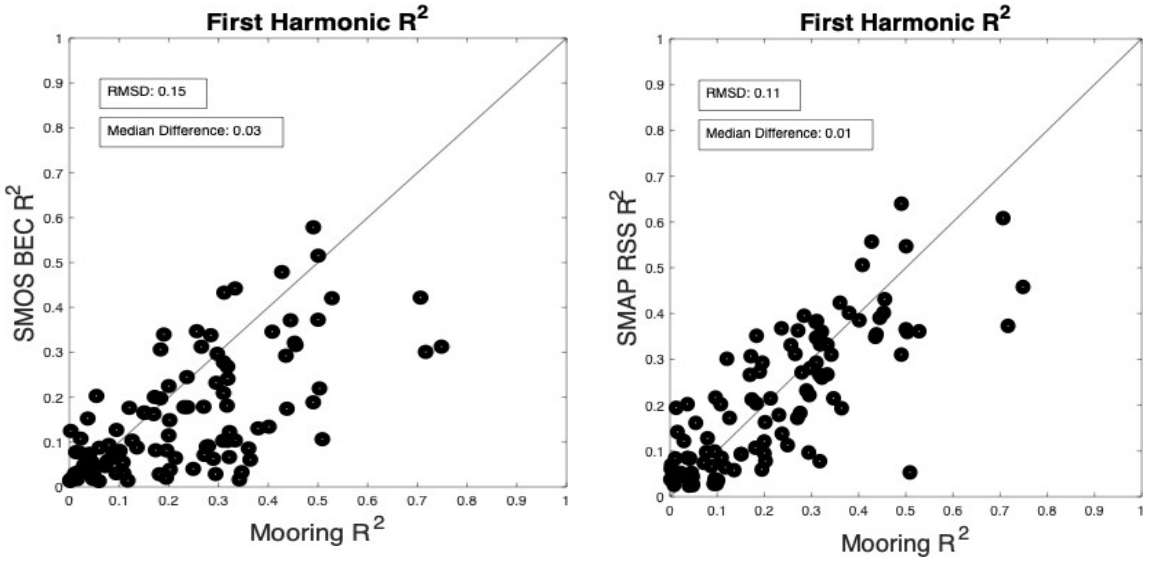

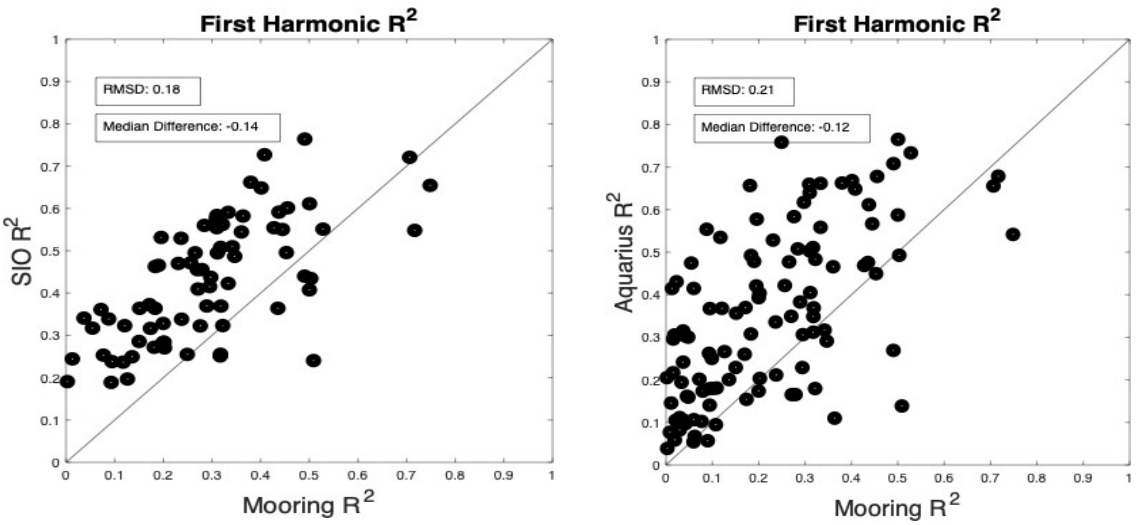

Figure 10. Scatterplots of fraction of variance, R^2, in the annual harmonic captured by four products, compared to that captured by the moorings. R^2 values are based on the entirety of each dataset, including possibly non-overlapping periods. Products are (a) SMOS BEC, (b) SMAP RSS, (c) SIO and (d) Aquarius.

4. Discussion

We have done comparisons of some various SSS datasets at the annual time scale. These comparisons are congruent with those of [18] among others. The advantage to our analysis is that it was done with the very long high-quality records of SSS at the moorings, and that these mooring data are largely independent of the products being evaluated. We have done more detailed comparisons of amplitude (Figure 8) and phase (Figure 6) in the discrete locations defined by the moorings (Figure 1) than was done by [18]. The disadvantage is the limited expanse of the mooring array – most are equatorward of 10° especially in the Pacific- and the limited spatial coverage of a point measurement from a mooring relative to the spatial averages from a satellite or gridded in situ product [33].

Most of the datasets record the phase of the annual cycle in a way that is reasonably consistent with the mooring data. Median phase differences between moorings and the products studied all include zero in their uncertainty range (Table 2, column 5 and Figure 7). The RMSD for phase between the moorings and the different products varies between 0.5 and 1.5 (Table 2, column 3 and Figure 7), giving an idea of the spread of phase values inherent in the data. Most of the products studied also give a reasonable value for the amplitude. Amplitude median differences are as high as 0.06 (Table 1, column 4), with some within the uncertainty range of zero.

It's difficult to track what exactly might be causing differences in products quantified in Table 2 given the variety of different processing algorithms, hardware configurations, antenna patterns, ancillary input data, etc. detailed in the references shown in Table S1. Are differences related to the conversion from L2 to L3? Is the annual cycle the same or similar in the L2 version of each of these as in the L3? Are any differences inherent in the hardware that is in orbit or are they part of the processing algorithm that converts engineering measurements within the satellite to geophysical measurements (L1 to L2)? Are they related to the footprint of the satellite or its antenna pattern? Its method of correcting for sea

state, Faraday rotation within the atmosphere, galaxy brightness, radio frequency interference filtering, etc.? We get some hint of the answers to these questions in the comparison of SMAP RSS and SMAP JPL (Figure 8a) and comparison of SMOS BEC and SMOS CATDS (Figure 8b). As these datasets originate from the same basic L1 observations, any differences must be related to the L1 to L2 or L2 to L3 conversion. In the case of SMAP, it appears that very little difference is introduced in the gridding and processing, but the opposite is the case with the SMOS datasets. Clearly answers to the questions posed in this paragraph will require more analysis.

Satellite SSS is usually validated against one of the common gridded in situ products [5, 7, 18, 34], of which we utilized two for our work here. As the seasonal time scale is one of the most energetic in terms of variability [19], it is important to make sure these products themselves are validated. We have done some of that here for a limited geographical extent and a very limited time scale – i.e. annual.

Most important for the process of validation is the different fractions of temporal variance captured in the annual time scale by the in situ products vs. the various satellite products (Table 3 and Figure 10). Given the fact that in situ products are mostly generated from sparse Argo data, it's expected that the seasonal time scale would be more heavily represented than anything shorter. Our results show however, that if validation is done using gridded products, important parts of the temporal spectrum of variability are missing. Do the satellite products get the balance correct between seasonal and shorter-term variability? Our results from Table 3 and Figure 10 show that this varies from one product to another.

As the moorings are a directly measured in situ dataset, the value of R^2 presented in Table 3 (0.19) likely is a good estimate of what fraction of variance the annual cycle represents in the real ocean – though Figure 10 indicates that this has a large degree of variation, from near-zero to almost 80%. A further extension on this study would be to use the mooring data to generate power spectra for each location to see how prominent the peaks are, and how those spectra compare with ones from the satellite data. A major difference between the satellite data and the moorings is the fact that the satellites measure over a footprint rather than at a point. One would expect this difference to reduce the variance in individual estimates of SSS and thus make spectral peaks, including a seasonal peak if present, more prominent. Table 3 shows that the fraction of variance in the mooring data is larger than one of the satellite datasets (SMOS BEC), comparable to most, and smaller than one (Aquarius). This seems a hopeful sign, that the satellite datasets are mostly doing well at capturing the seasonal cycle, or at least giving it the correct weight among the other time scales present in the ocean.

5. Conclusions

We have compared a variety of satellite and in situ products with SSS data from the GTMBA at the seasonal time scale. A summary of the important results of this paper is shown in Table 2, which gives RMSD and median difference (i.e. bias) for each product. The annual cycle is generally well-represented in all the products, though some discrepancies have been highlighted in the text. RMSD in amplitude (phase) has a range of 0.07-0.13 (0.5-1.5 months). Bias has a range of -0.02 - 0.06 (-0.1 - 0.1 months) in amplitude (phase). The different products have different characteristics with regards to the fraction of variance in the annual cycle (Table 3). Aquarius and the two in situ products have the largest fraction (up to 43%) and the SMOS BEC product the smallest (10%).

Supplementary Materials: The following are available online at [www.mdpi.com/xxx/s1], Tables S1-S7.

Author Contributions: Conceptualization: F.B. and L.Y.; formal analysis: S.B.; funding acquisition: F.B.; project administration: F.B.; software: F.B. and S.B.; supervision: F.B.; visualization: S.B.; writing – original draft: F.B.

402 and S.B.; writing – review & editing: F.B. and L.Y. All authors have read and agreed to the published version of
403 the manuscript.

404 **Funding:** This research was funded by the National Aeronautics and Space Administration under grant
405 number 80NSSC18K1322.

406 **Acknowledgments:** This study benefitted from comments given by NASA's Ocean Salinity Science Team.
407 SMAP salinity data are produced by Remote Sensing Systems and sponsored by the NASA Ocean Salinity
408 Science Team. They are available at www.remss.com. Color scales are taken from the "cmocean" package [35].

409 **Conflicts of Interest:** The authors declare no conflict of interest.

410

411 ## References

412 1. Kerr, Y.H.; Waldteufel, P.; Wigneron, J.P.; Delwart, S.; Cabot, F.; Boutin, J.; Escorihuela, M.J.; Font, J.;
413 Reul, N.; Gruhier, C., et al. The SMOS Mission: New Tool for Monitoring Key Elements of the Global
414 Water Cycle. Proceedings of the IEEE 2010, 98, 666-687, doi:10.1109/JPROC.2010.2043032.
415 2. Lagerloef, G.S.; Colomb, F.R.; Le Vine, D.M.; Wentz, F.; Yueh, S.; Ruf, C.; Lilly, J.; Gunn, J.; Chao, Y.;
416 deCharon, A., et al. The Aquarius/SAC-D Mission: Designed to Meet the Salinity Remote-sensing
417 Challenge. Oceanography 2008, 20, 68-81.
418 3. Meissner, T.; Wentz, F.; Le Vine, D. The salinity retrieval algorithms for the NASA Aquarius version 5
419 and SMAP version 3 releases. Remote Sensing 2018, 10, 1121, doi:10.3390/rs10071121.
420 4. Abe, H.; Ebuchi, N. Evaluation of sea−surface salinity observed by Aquarius. Journal of Geophysical
421 Research Oceans 2014, 119, 8109-8121, doi:10.1002/2014JC010094.
422 5. Bao, S.; Wang, H.; Zhang, R.; Yan, H.; Chen, J. Comparison of Satellite-Derived Sea Surface Salinity
423 Products from SMOS, Aquarius, and SMAP. Journal of Geophysical Research: Oceans 2019, 124, 1932-
424 1944, doi:10.1029/2019jc014937.
425 6. Vazquez-Cuervo, J.; Gomez-Valdes, J.; Bouali, M.; Miranda, L.E.; Van der Stocken, T.; Tang, W.;
426 Gentemann, C. Using Saildrones to Validate Satellite-Derived Sea Surface Salinity and Sea Surface
427 Temperature along the California/Baja Coast. Remote Sensing 2019, 11, doi:10.3390/rs11171964.
428 7. Kao, H.-Y.; Lagerloef, G.S.; Lee, T.; Melnichenko, O.; Meissner, T.; Hacker, P. Assessment of Aquarius Sea
429 Surface Salinity. Remote Sensing 2018, 10, 1341, doi:10.3390/rs10091341.
430 8. Kao, H.-Y.; Lagerloef, G.; Lee, T.; Melnichenko, O.; Hacker, P. Aquarius Salinity Validation Analysis;
431 Data Version 5.0; Aquarius/SAC-D: Seattle, 2018; p 45.
432 9. Olmedo, E.; Martínez, J.; Turiel, A.; Ballabrera-Poy, J.; Portabella, M. Debiased non-Bayesian retrieval: A
433 novel approach to SMOS Sea Surface Salinity. Remote Sensing of Environment 2017, 193, 103-126,
434 doi:10.1016/j.rse.2017.02.023.
435 10. Olmedo, E.; González-Haro, C.; Hoareau, N.; Umbert, M.; González-Gambau, V.; Martínez, J.; Gabarró,
436 C.; Turiel, A. Nine years of SMOS Sea Surface Salinity global maps at the Barcelona Expert Center. Earth
437 Syst. Sci. Data Discuss. 2020, 2020, 1-49, doi:10.5194/essd-2020-232.
438 11. Dinnat, E.P.; Le Vine, D.M.; Boutin, J.; Meissner, T.; Lagerloef, G. Remote Sensing of Sea Surface Salinity:
439 Comparison of Satellite and in situ Observations and Impact of Retrieval Parameters. Remote Sensing
440 2019, 11, 750, doi:10.3390/rs11070750.
441 12. Qin, S.; Wang, H.; Zhu, J.; Wan, L.; Zhang Y.; Wang H. Validation and correction of sea surface salinity
442 retrieval from SMAP. Acta Oceanologica Sinica, 2020, 39(3): 148–158, doi: 10.1007/s13131-020-1533-0
443 13. Roemmich, D.; Gilson, J. The 2004–2008 mean and annual cycle of temperature, salinity, and steric height
444 in the global ocean from the Argo Program. Progress in Oceanography 2009, 82, 81,
445 doi:10.1016/j.pocean.2009.1003.1004.
446 14. Kuusela, M.; Stein, M.L. Locally stationary spatio-temporal interpolation of Argo profiling float data.
447 Proc. R. Soc. A 2018, 474, doi:10.1098/rspa.2018.0400.
448 15. Bingham, F.M.; Foltz, G.R.; McPhaden, M.J. Seasonal cycles of surface layer salinity in the Pacific Ocean.
449 Ocean Science 2010, 6, 775-787, doi:10.5194/os-6-775-2010.
450 16. Bingham, F.M.; Foltz, G.R.; McPhaden, M.J. Characteristics of the Seasonal Cycle of Surface Layer Salinity
451 in the Global Ocean. Ocean Science 2012, 8, 915-929.
452 17. Boyer, T.P.; Levitus, S. Harmonic Analysis of Climatological Sea Surface Salinity. Journal of Geophysical
453 Research 2002, 107, 8006, doi:8010.1029/2001JC000829.
454 18. Yu, L.; Bingham, F.M.; Dinnat, E.; Fournier, S.; Lee, T.; Melnichenko, O. Seasonality in Sea Surface
455 Salinity Revisited. Journal of Geophysical Research Oceans 2020, in review.
456 19. Bingham, F.M.; Lee, T. Space and time scales of sea surface salinity and freshwater forcing variability in
457 the global ocean (60° S–60° N). Journal of Geophysical Research: Oceans 2017, 122, 2909-2922,
458 doi:10.1002/2016JC012216.
459 20. Sena Martins, M.; Serra, N.; Stammer, D. Spatial and temporal scales of sea surface salinity variability in
460 the Atlantic Ocean. Journal of Geophysical Research Oceans 2015, 120, 4306–4323,
461 doi:10.1002/2014JC010649.

21. Melnichenko, O.; Hacker, P.; Bingham, F.M.; Lee, T. Patterns of SSS Variability in the Eastern Tropical Pacific: Intraseasonal to Interannual Timescales from Seven Years of NASA Satellite Data. Oceanography 2019, 32, doi:10.5670/ oceanog.2019.208.
22. Kessler, W.S. The circulation of the eastern tropical Pacific: A review. Progress in Oceanography 2006, 69, 181-217, doi:10.1016/j.pocean.2006.03.009.
23. Guimbard, S.; Reul, N.; Chapron, B.; Umbert, M.; Maes, C. Seasonal and interannual variability of the Eastern Tropical Pacific Fresh Pool. Journal of Geophysical Research: Oceans 2017, 122, 1749-1771, doi:10.1002/2016JC012130.
24. Fiedler, P.C.; Talley, L.D. Hydrography of the eastern tropical Pacific: A review. Progress in Oceanography 2006, 69, 143-180, doi:10.1016/j.pocean.2006.03.008.
25. Foltz, G.R.; McPhaden, M.J. Seasonal Mixed Layer Salinity Balance of the Tropical North Atlantic Ocean. Journal of Geophysical Research.C.Oceans 2008, 113, C02013, doi:02010.01029/02007JC004178.
26. Grodsky, S.A.; Carton, J.A.; Bryan, F.O. A curious local surface salinity maximum in the northwestern tropical Atlantic. Journal of Geophysical Research: Oceans 2014, 119, 484-495, doi:10.1002/2013JC009450.
27. McPhaden, M.J.; Busalacchi, A.J.; Anderson, D.L.T. A TOGA Retrospective. Oceanography 2010, 23, 86-103, doi:10.5670/oceanog.2010.26.
28. Tang, W.; Yueh, S.H.; Fore, A.G.; Hayashi, A.; Lee, T.; Lagerloef, G. Uncertainty of Aquarius sea surface salinity retrieved under rainy conditions and its implication on the water cycle study. Journal of Geophysical Research: Oceans 2014, 119, 4821-4839, doi:10.1002/2014JC009834.
29. Tang, W.; Fore, A.; Yueh, S.; Lee, T.; Hayashi, A.; Sanchez-Franks, A.; Martinez, J.; King, B.; Baranowski, D. Validating SMAP SSS with in situ measurements. Remote Sensing of Environment 2017, 200, 326-340, doi:10.1016/j.rse.2017.08.021.
30. Meissner, T.; Wentz, F.; Manaseter, A. Remote Sensing Systems SMAP Ocean Surface Salinities Level 3 Running 8-day, Version 3.0 validated release. Systems, R.S., Ed. Remote Sensing Systems: Santa Rosa, CA, USA, 2018.
31. Drushka, K.; Asher, W.E.; Jessup, A.T.; Thompson, E.J.; Iyer, S.; Clark, D. Capturing Fresh Layers with the Surface Salinity Profiler. Oceanography 2019, 32, doi:10.5670/oceanog.2019.215.
32. D'Addezio, J.M.; Bingham, F.M.; Jacobs, G.A. Sea surface salinity subfootprint variability estimates from regional high-resolution model simulations. Remote Sensing of Environment 2019, 233, 111365, doi:10.1016/j.rse.2019.111365.
33. Bingham, F.M. Subfootprint Variability of Sea Surface Salinity Observed during the SPURS-1 and SPURS-2 Field Campaigns. Remote Sensing 2019, 11, 2689, doi:10.3390/rs11222689.
34. Fore, A.; Yueh, S.; Tang, W.; Hayashi, A. SMAP Salinity and Wind Speed Users Guide, Version 4.3; California Institute of Technology: Pasadena, CA, 2020; p 259.
35. Thyng, K.M.; Greene, C.A.; Hetland, R.D.; Zimmerle, H.M.; DiMarco, S.F. True Colors of Oceanography: Guidelines for Effective and Accurate Colormap Selection. Oceanography 2016, 29, 9-13, doi:10.5670/oceanog.2016.66.
36. Freitag, H.P.; McPhaden, M.J.; Connell, K.J. Comparison of ATLAS and T-FLEX Mooring Data; Pacific Marine Environmental Laboratory: Seattle, WA, 2018.
37. Olmedo, E.; González-Haro, C.; González-Gambau, V.; Martínez, J.; Turiel, A. Global SMOS-BEC SSS L3 and L4 Product V2 Description; Barcelona Expert Center: Barcelona, 2020.
38. Boutin, J.; Vergely, J.-L.; Thouvenin-Masson, C.; Supply, A.; Khvorostyanov, D. SMOS SSS L3 maps generated by CATDS CEC LOCEAN. debias V4.0. 4.0 ed.; Universite, S., Ed. 2019.
39. Boutin, J.; Vergely, J.L.; Marchand, S.; D'Amico, F.; Hasson, A.; Kolodziejczyk, N.; Reul, N.; Reverdin, G.; Vialard, J. New SMOS Sea Surface Salinity with reduced systematic errors and improved variability. Remote Sensing of Environment 2018, 214, 115-134, doi:10.1016/j.rse.2018.05.022.
40. Rouffi, F. Climate Change Initiative+ (CCI+) Phase 1: Sea Surface Salinity [D4.3] Product User Guide; ARGANS: 2020.
41. Fore, A.G.; Yueh, S.H.; Tang, W.; Stiles, B.W.; Hayashi, A.K. Combined Active/Passive Retrievals of Ocean Vector Wind and Sea Surface Salinity With SMAP. IEEE Transactions on Geoscience and Remote Sensing 2016, 54, 7396-7404, doi:10.1109/TGRS.2016.2601486.
42. Good, S.A.; Martin, M.J.; Rayner, N.A. EN4: Quality controlled ocean temperature and salinity profiles and monthly objective analyses with uncertainty estimates. Journal of Geophysical Research: Oceans 2013, 118, 6704-6716, doi:10.1002/2013JC009067.

517